

Measurement of CP Asymmetry in a Time-Dependent Dalitz Analysis of $B^0 \rightarrow (\rho\pi)^0$ and a Constraint on the Quark Mixing Matrix Angle ϕ_2

A. Kusaka,⁴⁷ C. C. Wang,²⁷ H. Ishino,⁴⁸ K. Abe,⁹ K. Abe,⁴⁵ I. Adachi,⁹ H. Aihara,⁴⁷ D. Anipko,¹ V. Aulchenko,¹ T. Aushev,^{19,14} A. M. Bakich,⁴² E. Barberio,²² A. Bay,¹⁹ I. Bedny,¹ K. Belous,¹³ U. Bitenc,¹⁵ I. Bizjak,¹⁵ S. Blyth,²⁵ A. Bondar,¹ A. Bozek,²⁸ M. Bračko,^{9,21,15} T. E. Browder,⁸ M.-C. Chang,⁴ P. Chang,²⁷ Y. Chao,²⁷ A. Chen,²⁵ K.-F. Chen,²⁷ W. T. Chen,²⁵ B. G. Cheon,⁷ R. Chistov,¹⁴ S.-K. Choi,⁶ Y. Choi,⁴¹ Y. K. Choi,⁴¹ S. Cole,⁴² J. Dalseno,²² M. Danilov,¹⁴ M. Dash,⁵¹ J. Dragic,⁹ A. Drutskoy,³ S. Eidelman,¹ S. Fratina,¹⁵ M. Fujikawa,²⁴ N. Gabyshev,¹ A. Garmash,³⁶ T. Gershon,⁹ G. Gokhroo,⁴³ B. Golob,^{20,15} H. Ha,¹⁷ J. Haba,⁹ T. Hara,³³ N. C. Hastings,⁴⁷ K. Hayasaka,²³ H. Hayashii,²⁴ M. Hazumi,⁹ D. Heffernan,³³ T. Hokuue,²³ Y. Hoshi,⁴⁵ S. Hou,²⁵ W.-S. Hou,²⁷ Y. B. Hsiung,²⁷ T. Iijima,²³ K. Ikado,²³ A. Imoto,²⁴ K. Inami,²³ A. Ishikawa,⁴⁷ R. Itoh,⁹ M. Iwasaki,⁴⁷ Y. Iwasaki,⁹ H. Kaji,²³ H. Kakuno,⁴⁷ J. H. Kang,⁵² P. Kapusta,²⁸ N. Katayama,⁹ H. Kawai,² T. Kawasaki,³⁰ H. R. Khan,⁴⁸ H. Kichimi,⁹ Y. J. Kim,⁵ K. Kinoshita,³ S. Korpar,^{21,15} P. Križan,^{20,15} P. Krokovny,⁹ R. Kulasiri,³ R. Kumar,³⁴ C. C. Kuo,²⁵ A. Kuzmin,¹ Y.-J. Kwon,⁵² J. Lee,³⁹ M. J. Lee,³⁹ S. E. Lee,³⁹ T. Lesiak,²⁸ A. Limosani,⁹ S.-W. Lin,²⁷ D. Liventsev,¹⁴ F. Mandl,¹² D. Marlow,³⁶ T. Matsumoto,⁴⁹ K. Miyabayashi,²⁴ H. Miyake,³³ Y. Miyazaki,²³ R. Mizuk,¹⁴ T. Mori,²³ E. Nakano,³² M. Nakao,⁹ H. Nakazawa,⁹ Z. Natkaniec,²⁸ S. Nishida,⁹ O. Nitoh,⁵⁰ S. Noguchi,²⁴ S. Ogawa,⁴⁴ T. Ohshima,²³ S. Okuno,¹⁶ Y. Onuki,³⁷ H. Ozaki,⁹ P. Pakhlov,¹⁴ G. Pakhlova,¹⁴ H. Park,¹⁸ K. S. Park,⁴¹ L. S. Peak,⁴² R. Pestotnik,¹⁵ L. E. Piilonen,⁵¹ A. Poluektov,¹ Y. Sakai,⁹ N. Satoyama,⁴⁰ O. Schneider,¹⁹ J. Schümamm,²⁶ A. J. Schwartz,³ R. Seidl,^{10,37} K. Senyo,²³ M. E. Seviar,²² M. Shapkin,¹³ H. Shibuya,⁴⁴ J. B. Singh,³⁴ A. Somov,³ N. Soni,³⁴ S. Stanič,³¹ M. Starič,¹⁵ H. Stoeck,⁴² S. Y. Suzuki,⁹ O. Tajima,⁹ F. Takasaki,⁹ K. Tamai,⁹ M. Tanaka,⁹ G. N. Taylor,²² Y. Teramoto,³² X. C. Tian,³⁵ I. Tikhomirov,¹⁴ K. Trabelsi,⁹ T. Tsuboyama,⁹ T. Tsukamoto,⁹ S. Uehara,⁹ T. Uglov,¹⁴ Y. Unno,⁷ S. Uno,⁹ P. Urquijo,²² Y. Ushiroda,⁹ Y. Usov,¹ G. Varner,⁸ S. Villa,¹⁹ C. H. Wang,²⁶ M.-Z. Wang,²⁷ Y. Watanabe,⁴⁸ R. Wedd,²² E. Won,¹⁷ Q. L. Xie,¹¹ B. D. Yabsley,⁴² A. Yamaguchi,⁴⁶ Y. Yamashita,²⁹ L. M. Zhang,³⁸ Z. P. Zhang,³⁸ V. Zhilich,¹ and A. Zupanc¹⁵

(The Belle Collaboration)

¹*Budker Institute of Nuclear Physics, Novosibirsk*

²*Chiba University, Chiba*

³*University of Cincinnati, Cincinnati, Ohio 45221*

⁴*Department of Physics, Fu Jen Catholic University, Taipei*

⁵*The Graduate University for Advanced Studies, Hayama, Japan*

⁶*Gyeongang National University, Chinju*

⁷*Hanyang University, Seoul*

⁸*University of Hawaii, Honolulu, Hawaii 96822*

⁹*High Energy Accelerator Research Organization (KEK), Tsukuba*

¹⁰*University of Illinois at Urbana-Champaign, Urbana, Illinois 61801*

¹¹*Institute of High Energy Physics, Chinese Academy of Sciences, Beijing*

¹²*Institute of High Energy Physics, Vienna*

¹³*Institute of High Energy Physics, Protvino*

¹⁴*Institute for Theoretical and Experimental Physics, Moscow*

¹⁵*J. Stefan Institute, Ljubljana*

¹⁶*Kanagawa University, Yokohama*

¹⁷*Korea University, Seoul*

¹⁸*Kyungpook National University, Taegu*

¹⁹*Swiss Federal Institute of Technology of Lausanne, EPFL, Lausanne*

²⁰*University of Ljubljana, Ljubljana*

²¹*University of Maribor, Maribor*

²²*University of Melbourne, Victoria*

²³*Nagoya University, Nagoya*

²⁴*Nara Women's University, Nara*

²⁵*National Central University, Chung-li*

²⁶*National United University, Miao Li*

²⁷*Department of Physics, National Taiwan University, Taipei*

²⁸*H. Niewodniczanski Institute of Nuclear Physics, Krakow*

- ²⁹*Nippon Dental University, Niigata*
³⁰*Niigata University, Niigata*
³¹*University of Nova Gorica, Nova Gorica*
³²*Osaka City University, Osaka*
³³*Osaka University, Osaka*
³⁴*Panjab University, Chandigarh*
³⁵*Peking University, Beijing*
³⁶*Princeton University, Princeton, New Jersey 08544*
³⁷*RIKEN BNL Research Center, Upton, New York 11973*
³⁸*University of Science and Technology of China, Hefei*
³⁹*Seoul National University, Seoul*
⁴⁰*Shinshu University, Nagano*
⁴¹*Sungkyunkwan University, Suwon*
⁴²*University of Sydney, Sydney NSW*
⁴³*Tata Institute of Fundamental Research, Bombay*
⁴⁴*Toho University, Funabashi*
⁴⁵*Tohoku Gakuin University, Tagajo*
⁴⁶*Tohoku University, Sendai*
⁴⁷*Department of Physics, University of Tokyo, Tokyo*
⁴⁸*Tokyo Institute of Technology, Tokyo*
⁴⁹*Tokyo Metropolitan University, Tokyo*
⁵⁰*Tokyo University of Agriculture and Technology, Tokyo*
⁵¹*Virginia Polytechnic Institute and State University, Blacksburg, Virginia 24061*
⁵²*Yonsei University, Seoul*

We present a measurement of CP asymmetry using a time-dependent Dalitz plot analysis of $B^0 \rightarrow \pi^+\pi^-\pi^0$ decays based on a 414fb^{-1} data sample containing $449 \times 10^6 B\bar{B}$ pairs. The data was collected on the $\Upsilon(4S)$ resonance with the Belle detector at the KEKB asymmetric energy e^+e^- collider. Combining our analysis with information on charged B decay modes, we perform a full Dalitz and isospin analysis and obtain a constraint on the CKM angle ϕ_2 , $68^\circ < \phi_2 < 95^\circ$ as the 68.3% confidence interval for the ϕ_2 solution consistent with the standard model (SM). A large SM-disfavored region also remains.

PACS numbers: 13.25.Hw, 11.30.Er, 12.15.Hh

In the standard model (SM), CP violation arises from an irreducible phase in the Cabibbo-Kobayashi-Maskawa (CKM) matrix [1, 2]. Snyder and Quinn pointed out that a time-dependent Dalitz plot analysis (TDPA) of the decay $B^0 \rightarrow \rho\pi \rightarrow \pi^+\pi^-\pi^0$ [3] offers a unique way to determine the angle ϕ_2 [4] in the CKM unitarity triangle without discrete ambiguities, which cannot be obtained from analyses of other modes sensitive to ϕ_2 such as $B \rightarrow \pi\pi$ or $\rho\rho$ [5]. The TDPA uses isospin and takes into account a possible contamination from $b \rightarrow d$ penguin transitions. In addition, using measurements of $B^+ \rightarrow$

$\rho^+\pi^0$ and $\rho^0\pi^+$ provides further improvement of the ϕ_2 determination [6, 7].

In this Letter, we present the result of a TDPA in $B^0 \rightarrow \pi^+\pi^-\pi^0$ decays and a constraint on ϕ_2 . We use a 414fb^{-1} data sample that contains $449 \times 10^6 B\bar{B}$ pairs collected on the $\Upsilon(4S)$ resonance. The data were taken at the KEKB collider [8] using the Belle detector [9].

In the decay chain $\Upsilon(4S) \rightarrow B^0\bar{B}^0 \rightarrow (\pi^+\pi^-\pi^0)f_{\text{tag}}$, where f_{tag} is a final state that distinguishes B^0 and \bar{B}^0 , the time- and Dalitz plot-dependent differential decay rate is

$$\frac{d\Gamma}{d\Delta t ds_+ ds_-} \sim e^{-|\Delta t|/\tau_{B^0}} \left\{ (|A_{3\pi}|^2 + |\bar{A}_{3\pi}|^2) - q_{\text{tag}} (|A_{3\pi}|^2 - |\bar{A}_{3\pi}|^2) \cos(\Delta m_d \Delta t) + q_{\text{tag}} \cdot 2\text{Im} \left[\frac{q}{p} A_{3\pi}^* \bar{A}_{3\pi} \right] \sin(\Delta m_d \Delta t) \right\}. \quad (1)$$

Here, $\bar{A}_{3\pi}$ is the Lorentz-invariant amplitude of the $B^0(\bar{B}^0) \rightarrow \pi^+\pi^-\pi^0$ decay, q_{tag} is the b -flavor charge ($q_{\text{tag}} = +1$ (-1) when f_{tag} is a B^0 (\bar{B}^0) flavor eigenstate), and Δt is the decay time difference of the two B mesons ($t_{3\pi} - t_{\text{tag}}$). The parameters p and q define the

mass eigenstates of neutral B mesons as $pB^0 \pm q\bar{B}^0$, with an average lifetime τ_{B^0} and mass difference Δm_d . The Dalitz plot variables s_+ , s_- , and s_0 are defined as

$$s_+ \equiv (p_+ + p_0)^2, \quad s_- \equiv (p_- + p_0)^2, \quad s_0 \equiv (p_+ + p_-)^2, \quad (2)$$

where p_+ , p_- , and p_0 are the four-momenta of the π^+ , π^- , and π^0 , respectively, in the decay of $B^0 \rightarrow \pi^+\pi^-\pi^0$.

The amplitudes $\overline{A}_{3\pi}$ have the following Dalitz plot dependences

$$A_{3\pi}(s_+, s_-) = \sum_{\kappa=(+,-,0)} f_{\kappa}(s_+, s_-) A^{\kappa}, \quad (3)$$

$$\frac{q}{p} \overline{A}_{3\pi}(s_+, s_-) = \sum_{\kappa=(+,-,0)} \overline{f}_{\kappa}(s_+, s_-) \overline{A}^{\kappa}, \quad (4)$$

where $A^{\kappa}(\overline{A}^{\kappa})$ are complex amplitudes corresponding to $B^0(\overline{B}^0) \rightarrow \rho^+\pi^-, \rho^-\pi^+, \rho^0\pi^0$ for $\kappa = +, -, 0$. Here we neglect possible contributions to the $B^0 \rightarrow \pi^+\pi^-\pi^0$ decay other than that of $B^0 \rightarrow (\rho\pi)^0 \rightarrow \pi^+\pi^-\pi^0$ and take account of them as systematic uncertainties. The functions \overline{f}_{κ} incorporate the kinematic and dynamical properties of $B^0 \rightarrow (\rho\pi)^0$ decays and can be written as

$$\overline{f}_{\kappa}(s_+, s_-) = T_{J=1}^{\kappa} \overline{F}_{\pi}^{\kappa}(s_{\kappa}) \quad (\kappa = +, -, 0), \quad (5)$$

where $T_{J=1}^{\kappa}$ and $\overline{F}_{\pi}^{\kappa}(s_{\kappa})$ correspond to the helicity dis-

tribution and the lineshape of ρ^{κ} , respectively. The lineshape is parameterized with Breit-Wigner functions corresponding to the $\rho(770)$ and its radial excitations:

$$\overline{F}_{\pi}^{\kappa}(s) = \text{BW}_{\rho(770)} + \overline{\beta}_{\kappa} \text{BW}_{\rho(1450)} + \overline{\gamma}_{\kappa} \text{BW}_{\rho(1700)}, \quad (6)$$

where the amplitudes $\overline{\beta}_{\kappa}$ and $\overline{\gamma}_{\kappa}$ (denoting the relative sizes of two resonances) are complex numbers. We use the Gounaris-Sakurai (GS) model [10] for the Breit-Wigner shape and the world average [11] for the mass and width of each resonance. Though $\overline{\beta}_{\kappa}$ and $\overline{\gamma}_{\kappa}$ can be different for each of six decay modes of $B^0(\overline{B}^0) \rightarrow (\rho\pi)^0$ in general, we assume no such variation, i.e., $\overline{\beta}_{\kappa} = \beta$ and $\overline{\gamma}_{\kappa} = \gamma$, in our nominal fit, and address possible deviations from this assumption in the systematic error. This assumption leads to the relation $\overline{f}_{\kappa}(s_+, s_-) = f_{\kappa}(s_+, s_-)$.

With this relation and Eqs. (3) and (4), the coefficients of Eq. (1) are

$$|A_{3\pi}|^2 \pm |\overline{A}_{3\pi}|^2 = \sum_{\kappa \in \{+, -, 0\}} |f_{\kappa}|^2 U_{\kappa}^{\pm} + 2 \sum_{\kappa < \sigma \in \{+, -, 0\}} (\text{Re}[f_{\kappa} f_{\sigma}^*] U_{\kappa\sigma}^{\pm, \text{Re}} - \text{Im}[f_{\kappa} f_{\sigma}^*] U_{\kappa\sigma}^{\pm, \text{Im}}), \quad (7)$$

$$\text{Im} \left(\frac{q}{p} A_{3\pi}^* \overline{A}_{3\pi} \right) = \sum_{\kappa \in \{+, -, 0\}} |f_{\kappa}|^2 I_{\kappa} + \sum_{\kappa < \sigma \in \{+, -, 0\}} (\text{Re}[f_{\kappa} f_{\sigma}^*] I_{\kappa\sigma}^{\text{Im}} + \text{Im}[f_{\kappa} f_{\sigma}^*] I_{\kappa\sigma}^{\text{Re}}), \quad (8)$$

with

$$U_{\kappa}^{\pm} = |A^{\kappa}|^2 \pm |\overline{A}^{\kappa}|^2, \quad (9)$$

$$I_{\kappa} = \text{Im} [\overline{A}^{\kappa} A^{\kappa*}], \quad (10)$$

$$U_{\kappa\sigma}^{\pm, \text{Re(Im)}} = \text{Re(Im)} [A^{\kappa} A^{\sigma*} \pm \overline{A}^{\kappa} \overline{A}^{\sigma*}], \quad (11)$$

$$I_{\kappa\sigma}^{\text{Re(Im)}} = \text{Re(Im)} [\overline{A}^{\kappa} A^{\sigma*} - (+) \overline{A}^{\sigma} A^{\kappa*}]. \quad (12)$$

The 27 coefficients (9)–(12) are the parameters determined by the fit [12]. The parameters (9)–(10) and (11)–(12) are called non-interfering and interfering parameters, respectively. This parameterization allows us to describe the differential decay width as a linear combination of independent functions, whose coefficients are fit parameters in a well behaved fit. We fix the overall normalization by requiring $U_{\pm}^{\pm} = 1$. Thus, 26 of the 27 coefficients are free parameters in the fit.

In contrast to a quasi-two-body CP violation analysis, a TDPA includes measurements of interfering parameters, which are measurements of CP -violating asymmetries in mixed final states. In principle, these measurements allow us to determine all the relative sizes and

phases of the amplitudes A^{κ} and \overline{A}^{κ} , which are related to ϕ_2 through an isospin relation [6, 7] by

$$e^{+2i\phi_2} = \frac{\overline{A}^+ + \overline{A}^- + 2\overline{A}^0}{A^+ + A^- + 2A^0}. \quad (13)$$

Consequently, in the limit of high statistics, we can constrain ϕ_2 without discrete ambiguities.

To reconstruct candidate $B^0 \rightarrow \pi^+\pi^-\pi^0$ decays, we combine pairs of oppositely charged tracks with π^0 candidates. The selection criteria for charged tracks are the same as in the previous $B^0 \rightarrow \rho^{\pm}\pi^{\mp}$ analysis [13]. Candidate π^0 's are reconstructed from γ pairs having $M_{\gamma\gamma}$ in the range 0.1178–0.1502 GeV/ c^2 , corresponding to ± 3 standard deviations (σ) in M_{π^0} resolution, and momenta greater than 0.1 GeV/ c in the laboratory frame. We require $E_{\gamma} > 0.05$ (0.1) GeV in the barrel (endcap) of the electromagnetic calorimeter [9], which subtends 32° – 129° (17° – 32° and 129° – 150°) with respect to the beam axis. Candidate B mesons are reconstructed using two variables calculated in the center-of-mass frame: the B invariant mass calculated using the beam energy in place

of the reconstructed energy (M_{bc}), and the energy difference between the B candidate and the beam energy (ΔE). We define a signal region $-0.1 \text{ GeV} < \Delta E < 0.08 \text{ GeV}$ and $5.27 \text{ GeV}/c^2 < M_{bc}$, and a large fitting region $|\Delta E| < 0.2 \text{ GeV}$ and $5.2 \text{ GeV}/c^2 < M_{bc}$.

The procedure used to measure Δt and to determine the flavor of the decaying B^0 meson, q_{tag} , and its quality, l , are described elsewhere [14]. The dominant background is $e^+e^- \rightarrow q\bar{q}$ ($q = u, d, s, c$) continuum events. To distinguish these jet-like events from the spherical B decay signal events, we combine modified Fox-Wolfram moments [15] and the B flight angle with respect to the beam direction into a signal (background) likelihood variable $\mathcal{L}_{\text{sig(bkg)}}$ and impose requirements on the likelihood ratio $\mathcal{R} \equiv \mathcal{L}_{\text{sig}}/(\mathcal{L}_{\text{sig}} + \mathcal{L}_{\text{bkg}})$. These requirements depend on the quality of flavor tagging. When more than one candidate in the same event is found in the large fitting region, we select the best candidate using likelihood based on $M_{\gamma\gamma}$ and \mathcal{R} . After the best candidate selection, we apply a Dalitz plot cut: candidates are required to satisfy $0.55 \text{ GeV}/c^2 < \sqrt{s_{\pm(0)}} < 1.0 (0.95) \text{ GeV}/c^2$ for at least one of s_+ , s_- , or s_0 . In the fits below, we use square Dalitz plot variables (m', θ') for convenience, performing a parameter transformation on (s_+, s_-) [16].

Figure 1 shows the M_{bc} (ΔE) distribution for the reconstructed $B^0 \rightarrow \pi^+\pi^-\pi^0$ candidates within the ΔE (M_{bc}) signal region. The signal yield is determined from an unbinned four-dimensional extended-maximum-likelihood fit to the ΔE - M_{bc} and Dalitz plot distribution in the large fitting region, where the Dalitz plot distribution is fitted only for events inside the ΔE - M_{bc} signal region. The fit function includes signal; incorrectly reconstructed signal, which we call self-cross-feed (SCF); continuum; and $B\bar{B}$ background components. The probability density function (PDF) for each component is the same as that used for the TDPA described below, but integrated over Δt and summed over q_{tag} . The fit yields $971 \pm 42 B^0 \rightarrow \pi^+\pi^-\pi^0$ events in the signal region, where the errors are statistical only.

Using the same data sample as described above but

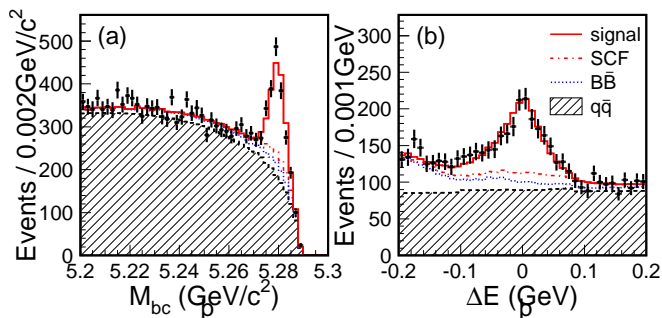


FIG. 1: (a) M_{bc} and (b) ΔE distributions within the ΔE and M_{bc} signal regions. Solid, dot-dashed, dotted, and dashed hatched histograms correspond to correctly reconstructed signal, SCF, $B\bar{B}$, and continuum PDF's, respectively.

performing a time-integrated Dalitz plot fit with a wider Dalitz plot acceptance, $0.0 (0.55) \text{ GeV}/c^2 < \sqrt{s_{\pm(0)}} < 1.5 \text{ GeV}/c^2$, we determine the ρ lineshape parameters β and γ . We use the results obtained for the TDPA below. We also put upper limits on the possible deviations of $(\bar{\beta}_\kappa, \bar{\gamma}_\kappa)$ from the nominal (β, γ) , which we use to estimate systematic errors.

To determine the 26 coefficients, we define the following event-by-event PDF:

$$P = \sum_{X=\text{sig}, q\bar{q}, B\bar{B}} f_X \mathcal{P}_X(\Delta E, M_{bc}, m', \theta', \Delta t, q_{\text{tag}}, l),$$

where \mathcal{P}_{sig} , $\mathcal{P}_{q\bar{q}}$, and $\mathcal{P}_{B\bar{B}}$ are the PDF's of signal including SCF, continuum, and $B\bar{B}$ components, respectively, and f_{sig} , $f_{q\bar{q}}$, and $f_{B\bar{B}}$ are the corresponding fractions that satisfy $f_{\text{sig}} + f_{q\bar{q}} + f_{B\bar{B}} = 1$. Here, \mathcal{P}_{sig} and $\mathcal{P}_{B\bar{B}}$ are modeled based on Monte Carlo (MC), though a small correction is applied to \mathcal{P}_{sig} to take account of the difference between data and MC, while $\mathcal{P}_{q\bar{q}}$ is modeled using data. The signal PDF, \mathcal{P}_{sig} , is the sum of a correctly reconstructed PDF ($\mathcal{P}_{\text{true}}$) and an SCF PDF, where

$$\begin{aligned} \mathcal{P}_{\text{true}} = & \mathcal{F}_{\text{true}}^l \mathcal{P}_{\text{true}}(\Delta E, M_{bc}) \epsilon(m', \theta'; l) \\ & \times \mathcal{P}_{\text{true}}(m', \theta', \Delta t, q_{\text{tag}}; l). \end{aligned}$$

Here $\mathcal{F}_{\text{true}}^l$, $\mathcal{P}_{\text{true}}(\Delta E, M_{bc})$, $\epsilon(m', \theta'; l)$, and $\mathcal{P}_{\text{true}}(m', \theta', \Delta t, q_{\text{tag}}; l)$ are event fractions in each category of tagging quality l , a ΔE - M_{bc} PDF, a Dalitz plot dependent efficiency, and a Dalitz- Δt PDF for the correctly reconstructed signal component, respectively. The Dalitz- Δt PDF corresponds to the right-hand side of Eq. (1) with the following modifications: (i) it is convolved with the Δt resolution function [17]; (ii) it is multiplied by the determinant of the Jacobian for the transformation $(s_+, s_-) \mapsto (m', \theta')$; and (iii) the wrong tag fractions, w_l , and the difference between B^0 and \bar{B}^0 decays, Δw_l , are taken into account. A more detailed description of the PDF can be found elsewhere [18].

An unbinned-maximum-likelihood fit to the 2824 events in the signal region yields the results listed in Table I. With a toy MC study, we find that the errors estimated by the likelihood function do not give correct 68.3% confidence level (C.L.) coverage for the interfering parameters. In the table, we multiply the error estimates from the likelihood function by a factor of 1.17, which is calculated from the MC study, to obtain errors with correct coverage. We find that U_0^+ is 4.8σ above zero, corresponding to clear evidence for the presence of the decay $B^0 \rightarrow \rho^0\pi^0$ in agreement with our previous measurement [19]. Figure 2 shows the mass and helicity distributions, and the background-subtracted Δt asymmetry plot for each $\rho\pi$ enhanced region. We define the asymmetry in each Δt bin by $(N_+ - N_-)/(N_+ + N_-)$, where $N_{+(-)}$ corresponds to the background-subtracted number of events with $q_{\text{tag}} = +1 (-1)$. The $\rho^-\pi^+$ enhanced region shows a significant cosine-like asymmetry

TABLE I: Results of the time-dependent Dalitz fit (left three columns), and the associated quasi-two-body CP violation parameters (rightmost column), whose definitions can be found elsewhere [13]. The first and second errors are statistical and systematic, respectively. The correlation coefficient between $\mathcal{A}_{\rho\pi}^{+-}$ and $\mathcal{A}_{\rho\pi}^{-+}$ ($\mathcal{A}_{\rho^0\pi^0}$ and $\mathcal{S}_{\rho^0\pi^0}$) is $+0.47$ (-0.08).

U_+^+	+1 (fixed)	U_-^-	$+0.23 \pm 0.15 \pm 0.07$	I_+	$-0.01 \pm 0.11 \pm 0.04$	$\mathcal{A}_{\rho\pi}^{CP}$	$-0.12 \pm 0.05 \pm 0.04$
U_-^+	$+1.27 \pm 0.13 \pm 0.09$	U_-^-	$-0.62 \pm 0.16 \pm 0.08$	I_-	$+0.09 \pm 0.10 \pm 0.04$	\mathcal{C}	$-0.13 \pm 0.09 \pm 0.05$
U_0^+	$+0.29 \pm 0.05 \pm 0.04$	U_0^-	$+0.15 \pm 0.11 \pm 0.08$	I_0	$+0.02 \pm 0.09 \pm 0.05$	$\Delta\mathcal{C}$	$+0.36 \pm 0.10 \pm 0.05$
$U_{+-}^{+,Re}$	$+0.49 \pm 0.86 \pm 0.52$	$U_{+-}^{-,Re}$	$-1.18 \pm 1.61 \pm 0.72$	I_{+-}^{Re}	$+1.21 \pm 2.59 \pm 0.98$	\mathcal{S}	$+0.06 \pm 0.13 \pm 0.05$
$U_{+0}^{+,Re}$	$+0.29 \pm 0.50 \pm 0.35$	$U_{+0}^{-,Re}$	$-2.37 \pm 1.36 \pm 0.60$	I_{+0}^{Re}	$+1.15 \pm 2.26 \pm 0.92$	$\Delta\mathcal{S}$	$-0.08 \pm 0.13 \pm 0.05$
$U_{-0}^{+,Re}$	$+0.25 \pm 0.60 \pm 0.33$	$U_{-0}^{-,Re}$	$-0.53 \pm 1.44 \pm 0.65$	I_{-0}^{Re}	$-0.92 \pm 1.34 \pm 0.80$	$\mathcal{A}_{\rho\pi}^{+-}$	$+0.21 \pm 0.08 \pm 0.04$
$U_{+-}^{+,Im}$	$+1.18 \pm 0.86 \pm 0.34$	$U_{+-}^{-,Im}$	$-2.32 \pm 1.74 \pm 0.91$	I_{+-}^{Im}	$-1.93 \pm 2.39 \pm 0.89$	$\mathcal{A}_{\rho\pi}^{-+}$	$+0.08 \pm 0.16 \pm 0.11$
$U_{+0}^{+,Im}$	$-0.57 \pm 0.35 \pm 0.51$	$U_{+0}^{-,Im}$	$-0.41 \pm 1.00 \pm 0.47$	I_{+0}^{Im}	$-0.40 \pm 1.86 \pm 0.85$	$\mathcal{A}_{\rho^0\pi^0}$	$-0.49 \pm 0.36 \pm 0.28$
$U_{-0}^{+,Im}$	$-1.34 \pm 0.60 \pm 0.47$	$U_{-0}^{-,Im}$	$-0.02 \pm 1.31 \pm 0.83$	I_{-0}^{Im}	$-2.03 \pm 1.62 \pm 0.81$	$\mathcal{S}_{\rho^0\pi^0}$	$+0.17 \pm 0.57 \pm 0.35$

arising from a non-zero value of U_-^- . Note that this is not a CP -violating effect, since $\rho^-\pi^+$ is not a CP -eigenstate. No sine-like asymmetry is observed in any of the regions (g)–(i).

The non-interfering parameters can be interpreted as the quasi-two-body parameters of the process $B^0 \rightarrow \rho^\pm\pi^\mp$, whose definitions can be found elsewhere [13], and the CP violation parameters of the process $B^0 \rightarrow \rho^0\pi^0$: $\mathcal{A}_{\rho^0\pi^0} = -U_0^-/U_0^+$ and $\mathcal{S}_{\rho^0\pi^0} = 2I_0/U_0^+$. These are also listed in the Table I.

There are several sources of systematic uncertainty. To determine their magnitudes, we vary each possible contribution to the systematic error by its uncertainty in the data fit or in the MC, and take the resultant deviations in the fitted parameters as errors. We add each contribution in quadrature to obtain the total systematic uncertainty. The largest contribution for the interfering parameters comes from radial excitations. We take account of pos-

sible deviations of $(\overline{\beta}_\kappa, \overline{\gamma}_\kappa)$ from the (β, γ) values, and uncertainties of β, γ , and the mass and width of each resonance. Large contributions to the systematic errors for the non-interfering parameters come from potential backgrounds such as $B^0 \rightarrow f_0(980)\pi^0, f_0(600)\pi^0, \omega\pi^0$, and non-resonant $\pi^+\pi^-\pi^0$, which we neglect in our nominal fit. We perform fits to toy MC including these backgrounds with the branching fractions at their 68.3% C.L. upper limits, which we obtain from our data or world averages [11, 20]; the largest variations are taken as systematic errors. Comparable contributions also come from vertex reconstruction, background PDF's, and tag-side interference [21]; more detail can be found elsewhere [18].

We constrain ϕ_2 from the 26 parameters measured in our analysis following the formalism of Ref. [5] and the statistical treatment using toy MC described in Ref. [22]. The resulting $1 - \text{C.L.}$ function is shown in Fig. 3 as a dotted curve. To incorporate all available knowledge, we combine our measurement with results on the branching fractions for $B^0 \rightarrow \rho^\pm\pi^\mp$ and $B^+ \rightarrow \rho^+\pi^0, \rho^0\pi^+$, and flavor asymmetries of the latter two [20]. Assuming isospin (pentagon) relations [6, 7] and following the same procedure as above, we perform a full Dalitz and pentagon combined analysis, the result of which is shown in Fig. 3 as the solid curve. We obtain $68^\circ < \phi_2 < 95^\circ$ as the 68.3% confidence interval for the solution consistent

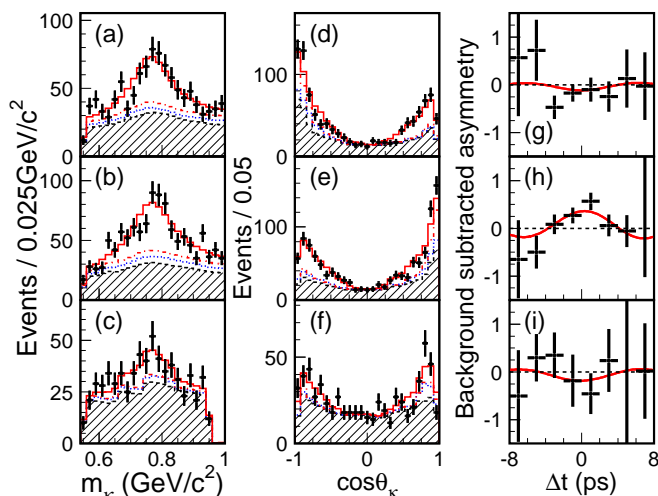


FIG. 2: Mass (a)–(c) and helicity (d)–(f) distributions, and background subtracted Δt asymmetry plots in the good tagging quality region $l \geq 3$ [14] (g)–(i), corresponding to the $\rho^+\pi^-$ [(a),(d),(g)], $\rho^-\pi^+$ [(b),(e),(h)], and $\rho^0\pi^0$ [(c),(f),(i)] enhanced regions. The notations for histograms (a)–(f) are the same as Fig. 1.

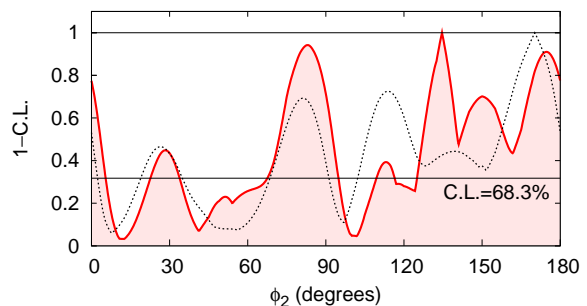


FIG. 3: $1 - \text{C.L.}$ vs. ϕ_2 . Dotted and solid curves correspond to the result from the TDPA only and that from the TDPA and an isospin (pentagon) combined analysis, respectively.

with the SM expectation. A large SM-disfavored region ($0^\circ < \phi_2 < 5^\circ$, $23^\circ < \phi_2 < 34^\circ$, and $109^\circ < \phi_2 < 180^\circ$) also remains. In principle, with more data we may be able to remove the additional ϕ_2 solutions.

In summary, using 414 fb^{-1} of data we have performed a full Dalitz plot analysis of the $B^0 \rightarrow \pi^+\pi^-\pi^0$ decay mode, where the observables include the first measurement of $\mathcal{S}_{\rho^0\pi^0}$. A full time-dependent Dalitz plot analysis with the pentagon isospin relation is performed for the first time and a constraint on the angle ϕ_2 is obtained.

We thank the KEKB group for excellent operation of the accelerator, the KEK cryogenics group for efficient solenoid operations, and the KEK computer group and the NII for valuable computing and Super-SINET network support. We acknowledge support from MEXT and JSPS (Japan); ARC and DEST (Australia); NSFC and KIP of CAS (China); DST (India); MOEHRD, KOSEF and KRF (Korea); KBN (Poland); MIST (Russia); ARRS (Slovenia); SNSF (Switzerland); NSC and MOE (Taiwan); and DOE (USA).

[1] N. Cabibbo, Phys. Rev. Lett. **10**, 531 (1963).

[2] M. Kobayashi and T. Maskawa, Prog. Theor. Phys. **49**, 652 (1973).

[3] Throughout this Letter, the inclusion of the charge conjugate decay mode is implied unless otherwise stated.

[4] Another naming convention, α ($= \phi_2$), is also used in the literature.

[5] A. E. Snyder and H. R. Quinn, Phys. Rev. D **48**, 2139 (1993). We assume ϕ_2 is in the range between 0 and π .

[6] H. J. Lipkin, Y. Nir, H. R. Quinn, and A. E. Snyder,

Phys. Rev. D **44**, 1454 (1991).

[7] M. Gronau, Phys. Lett. B **265**, 389 (1991).

[8] S. Kurokawa and E. Kikutani, Nucl. Instrum. Meth. A **499**, 1 (2003), and other papers included in this volume.

[9] A. Abashian *et al.* (Belle Collaboration), Nucl. Instrum. Meth. A **479**, 117 (2002).

[10] G. J. Gounaris and J. J. Sakurai, Phys. Rev. Lett. **21**, 244 (1968).

[11] S. Eidelman *et al.* (Particle Data Group), Phys. Lett. B **592**, 1 (2004), and 2005 partial update (<http://pdg.lbl.gov>). For the uncertainties in the masses and widths of the $\rho(1450)$ and $\rho(1700)$, we use twice the errors quoted in the references above.

[12] H. R. Quinn and J. P. Silva, Phys. Rev. D **62**, 054002 (2000).

[13] C. C. Wang *et al.* (Belle Collaboration), Phys. Rev. Lett. **94**, 121801 (2005).

[14] K. F. Chen *et al.* (Belle Collaboration), Phys. Rev. D **72**, 012004 (2005).

[15] K. Abe *et al.* (Belle Collaboration), Phys. Rev. Lett. **91**, 261801 (2003).

[16] B. Aubert *et al.* (BaBar Collaboration), Phys. Rev. D **72**, 052002 (2005).

[17] H. Tajima *et al.*, Nucl. Instrum. Meth. A **533**, 370 (2004).

[18] K. Abe *et al.* (Belle Collaboration) (2006), hep-ex/0609003.

[19] J. Dragic *et al.* (Belle Collaboration), Phys. Rev. D **73**, 111105 (2006).

[20] E. Barberio *et al.* (Heavy Flavor Averaging Group (HFAG)) (2006), hep-ex/0603003; and online update of Summer 2006 (<http://www.slac.stanford.edu/xorg/hfag>).

[21] O. Long, M. Baak, R. N. Cahn, and D. Kirkby, Phys. Rev. D **68**, 034010 (2003).

[22] J. Charles *et al.* (CKMfitter Group), Eur. Phys. J. C **41**, 1 (2005).